Position Control Study of a Bearingless Multi-Sector Permanent Magnet Machine

G. Valente
Uni. of Nottingham
Nottingham, Uk
giorgio.valente@nottingham.ac.uk

A. Formentini
Uni. of Nottingham
Nottingham, Uk

L. Papini
Uni. of Nottingham
Nottingham, Uk

P. Zanchetta
Uni. of Nottingham
Nottingham, Uk

C. Gerada
Uni. of Nottingham
Nottingham, Uk

***Abstract*—Bearingless motors combine in the same structure the characteristics of conventional motors and magnetic bearings. Traditional bearingless machines rely on two independent sets of winding for suspension force and torque production, respectively. The proposed Multi-Sector Permanent Magnet (MSPM) motor exploits the spatial distribution of the multi-three-phase windings within the stator circumference in order to produce a controllable suspension force. Therefore, force and torque generation are embedded in the same winding setting. In this paper the force and torque generation principles are investigated and a mathematical model is presented considering the rotor displacement. A two Degree of freedom (DOF) position controller is designed taking into consideration the rotor overall dynamic system and a controller gains selection strategy is suggested. A simulation study of the bearingless system in different operating conditions is presented and the suspension force and torque produced are validated through Finite Element Analysis (FEA).**

***Index Terms*—Bearingless machines, Multi-Sector Permanent Magnet machines, Radial Force Control.**

I. Introduction

In the last two decades, Bearingless Permanent Magnet BPM motors have being intensively investigated and continuously developed and improved thanks to the progress of high-energy PM materials, power electronic technology, digital signal processing technology, and modern control theory [1]. A full levitating system is particularly convenient when ultra-high rotation speeds have to be achieved [2]. It is the case of compressors, spindles, flywheels [3] and generators where high rotational speed operation means minimize the weight, dimensions and cost, and maximize the efficiency of the whole system [4].

The full rotor dynamic control of the rotating component can be achieved suspending the rotor element by mean a combination of Active Magnetic Bearings (AMBs) and Passive magnetic Bearings (PMBs) while the electrical machine is typically designed to optimize the torque production [5]. This solution consists in a rather bulky and complex structure since several electric machines are required to stably suspend and rotate the rotor. Consequently, bearingless PMSM technology has been proposed more recently in order to embed the characteristic of AMBs and PMBs into the motor structure. As a matter of facts, BPM motors allows enhancing the reliability, maximizing the power to weight ratio as well as the power to volume ratio .

In [6] the x-y forces and the torque developed by the electrical motor are independently controlled adopting two sets of windings with different pole pairs. Therefore, an additional winding for force production is installed in the BPM motor leading to a bigger outer diameter than that of the conventional motor. A different approach has been investigated in [7] where lateral forces are produced with a conventional three-phase winding where each phase current that produces torque is divided into two parallel paths. A small power converter connected between mid-points of each path provides the current responsible for the lateral force production. In [8], the force and torque produced in a multiphase slice permanent magnet bearingless motor are controlled by solving an optimization problem that minimizes the power losses in the machine. In [9], the geometrical arrangement of the winding structure, formed by three winding sectors, enables the control of the torque as well as the net radial force through the independent $d-q$ axis current control of each sector. In [10], an alternative radial force and torque control is applied to a MSPM motor consisting in a conventional surface PMSM but with a re-arranged winding configuration. The mathematical model developed describes an efficient radial force and torque control technique where the cross-coupling effects in the force and torque capabilities of the system are taken into account.

In the proposed work, the mathematical model presented in [10] has been extended to take the rotor radial displacement into account. Then, the rotor dynamic system has been introduced and a 2-DOF position controller is designed. The controller parameters are set in order to guarantee stable rotor suspension under different kind of disturbances. Finally, a simulation system is prepared using the MATLAB-Simulink environment in order to simulate different operating conditions and the resultant suspension force components and torque are validated through the comparison with FE results.

II. The Electro-mechanical Characterization of the MSPM Motor

This section deals with the electromagnetic characterization of the MSPM motor considered. At first, a brief description of the force production principles for the considered MSPM machine will be provided. Then a mathematical model that describes the current to x-y force and torque relation will be described. The model is derived in a generic form that can be extended to every MSPM machine and takes into account for

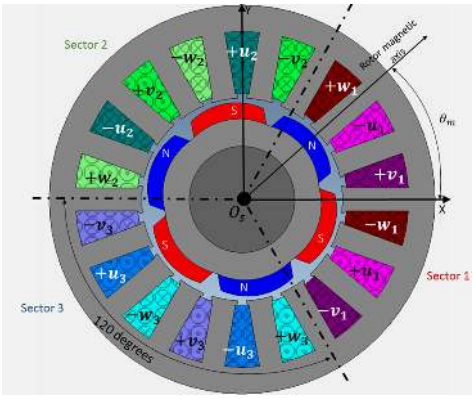

Fig. 1. Cross section of the 18 slot - 6 poles - 3 sectors MSPM motor considered.

TABLE I
MACHINE PARAMETERS

Parameter	Value
Pole number ($2p$)	6
Rotor mass m	2 [Kg]
Power rating	1.5 [kW]
Nominal current peak I_n	13 [A]
Rated Speed (ω_m)	3000 [rpm]
Torque constant (k_T)	0.128 [Nm/A]
Line to line voltage constant (k_V)	15.5 [V/krpm]
Outer Stator diameter	95 [mm]
Inner Stator diameter	49.5 [mm]
Axial length L	90 [mm]
Airgap length g_0	1 [mm]

the rotor radial displacement.
Finally, an energy efficient strategy that provides the current commands required to control the x-y force and torque will be given.

A. The machine structure and force production principle

Fig. 1 shows the cross section and the multi-three phase winding arrangement of the MSPM motor while the main characteristics are listed in Table I. The left superscript s in this manuscript will be adopted in order to define quantities related to the single s^{th} sector. The machine under investigation has a number of sectors $n_s = p$, each of them composed by a full-pitched distributed winding with a floating star point. The angular position of the generic sector s with respect the x-axis is given by ${}^s\gamma = s\,(2\pi)/n_s + \gamma_0$ where γ_0 defines the angular position of the magnetic axis of the sector 1.
The torque generation principles are the same of a standard three-phase motor with the only difference that each sector contributes to $1/n_s$ of the total torque. Furthermore, the independent current control of each sector allows to unbalance the flux density distribution of the airgap producing a net radial force. As a matter of fact, strengthening the flux density in the airgap underneath sector 1 and weakening the ones in correspondence of sector 2 and 3 produces a resultant force along the $x-$ axis direction.

B. The mathematical model

The mathematical model that will be presented in this section is based on the following assumptions: linear magnetic behaviour of the materials and magnetic decoupling between sectors. Furthermore, the rotor is considered a rigid body that is allowed to move radially within a certain displacement δ_{max} given by the clearance of the backup bearing. Hence, the mathematical model will take into account the rotor radial displacement defined by the translation δ and angle φ_d of the rotor centre from the rectangular $x-y$ reference frame origin of the stator O_s. Under the above mentioned assumptions the matrix formulation (1) expresses the generalized mechanical wrench of the motor [11] as a function of the electrical angular position $\vartheta_e = p\vartheta_m$ and radial displacement of the rotor and stationary reference frame current components ${}^s i_\alpha$ and ${}^s i_\beta$ of each sector s.

$$\bar{W}_E = \mathbf{K}_E(\vartheta_e, {}^s\gamma)\bar{I}_{\alpha\beta} + \bar{K}_m(\varphi_d)\delta \tag{1}$$

Where $\bar{W}_E = \begin{bmatrix} F_x(\vartheta_e) & F_y(\vartheta_e) & T(\vartheta_e) \end{bmatrix}^T$ is the mechanical $x-y$ forces and torque vector and $\bar{I}_{\alpha\beta} = \begin{bmatrix} {}^1i_\alpha & {}^1i_\beta & \cdots & {}^s i_\alpha & {}^s i_\beta & \cdots & {}^{n_s} i_\alpha & {}^{n_s} i_\beta \end{bmatrix}^T$ is the total vector of the $\alpha-\beta$ axis currents. Matrix $\mathbf{K}_E(\vartheta_e, {}^s\gamma) \in \mathbb{R}^{3\times 2n_s}$ contains the force and torque coefficients that link the $\alpha-\beta$ current quantities to the mechanical x-y force and torque outputs. Its structure is reported in (2).

$$\boldsymbol{K}_E = \begin{bmatrix} {}^1\boldsymbol{K}_E(\vartheta_e, {}^1\gamma) & \cdots & {}^{n_s}\boldsymbol{K}_E(\vartheta_e, {}^{n_s}\gamma) \end{bmatrix} \tag{2}$$

Matrix ${}^s\mathbf{K}_E(\theta_e, {}^s\gamma) \in \mathbb{R}^{3\times 2}$ can be written in (3) explicating the sub-matrix ${}^s\mathbf{K}_{E,F}(\theta_e, {}^s\gamma) \in \mathbb{R}^{2\times 2}$ and sub-matrix ${}^s\bar{K}_{E,T}(\vartheta_e) \in \mathbb{R}^{1\times 2}$ of the force and torque coefficients, respectively.

$${}^s\mathbf{K}_E(\vartheta_e, {}^s\gamma) = \begin{bmatrix} {}^s\mathbf{K}_{E,F}(\vartheta_e, {}^s\gamma) \\ {}^s\bar{K}_{E,T}(\vartheta_e) \end{bmatrix} \tag{3}$$

Each motor sector presents an identical sub-matrix ${}^s\mathbf{K}_{E,T}(\theta_e)$ as the torque coefficients only depend on the torque constant k_T and rotor angular position ϑ_e. On the contrary, sub-matrix ${}^s\mathbf{K}_{E,F}(\vartheta_e, {}^s\gamma)$ is also a function of the angle ${}^s\gamma$, hence it has to be determined for each sector s. However, exploiting the geometrical symmetries of the MSPM motor considered only one sub-matrix ${}^s\mathbf{K}_{E,F}(\vartheta_e, {}^s\gamma)$ can be characterized and the other $n_s - 1$ can be derived accordingly. In [12] sub-matrix ${}^1\mathbf{K}_{E,F}(\vartheta_e, {}^1\gamma)$ (with ${}^1\gamma = 0$) has been characterized both analytically and through FE simulations and the remaining $n_s - 1$ are obtained as follow.

$${}^s\mathbf{K}_E(\vartheta_e, {}^s\gamma) = \mathbf{R}({}^s\gamma)\,{}^1\mathbf{K}_E(\vartheta_e, 0) \tag{4}$$

Where $\mathbf{R}({}^s\gamma)$ is an appropriate rotating matrix defined in [10]. Finally, $\bar{K}_m(\varphi_d)$, expressed in (5), is the magnetic stiffness vector of the motor.

$$\bar{K}_m(\varphi_d) = \begin{bmatrix} k_m\cos(\varphi_d) \\ k_m\sin(\varphi_d) \\ 0 \end{bmatrix} \tag{5}$$

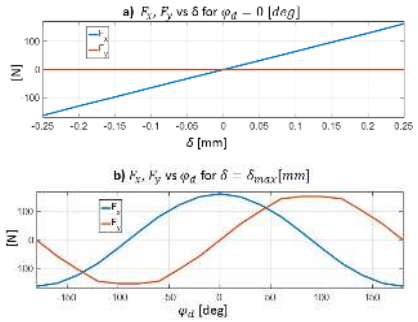

Fig. 2. Open circuit forces as a function of the rotor displacement variables δ and φ_d.

Where k_m is the magnetic stiffness constant. The first two components of $\bar{K}_m(\varphi_d)$ can be justified observing Fig. 2 where the open circuit $x-y$ force components trend as a function of δ and φ_d is shown. Fig. 2 a) and 2 b) have been obtained running two 2D "multi-static" FE simulations varying the values of δ and of φ_d, respectively. A maximum displacement of $\delta_{max} = 0.25[mm]$ (25% of the airgap g_0) has being chosen in order to fulfil the force capability of the motor. As a matter of fact, the amplitude of the open circuit force at δ_{max} is around 165[N], corresponding to almost 90% of the force capability of the motor. It is straightforward to notice that the trend of the force vs δ is linear, hence the stiffness constant can be obtained as $k_m = 165/\delta_{max} = 660000[N/m]$ [12]. The last component of $\bar{K}_m(\varphi_d)$ is zero meaning that the average torque is not significantly affected by the rotor displacement in the range considered.

C. The current reference calculation strategy

The problem of calculating the current command can be solved inverting matrix $\mathbf{K}_E$. However, $\mathbf{K}_E$ results in general in a rectangular matrix, hence it cannot be easily inverted. In [10] the minimization of the copper losses has been chosen as strategy leading to the calculation of the pseudo inverse of $\mathbf{K}_E$ as follow.

$$\mathbf{K}_E^{+} = \mathbf{K}_E^T(\mathbf{K}_E\mathbf{K}_E^T)^{-1} \tag{6}$$

Therefore, the current command $\bar{I}^*_{\alpha\beta}$ can be calculated in (7) considering also the rotor displacement.

$$\bar{I}^*_{\alpha\beta} = \mathbf{K}_E^{+}\big(\bar{W}^*_E - \bar{K}_m(\varphi_d)\delta\big) = \mathbf{K}_E^{+}\big(\bar{W}^*_E - k_m \begin{bmatrix} u \\ v \\ 0 \end{bmatrix}\big) \tag{7}$$

Where u and v are the $x-$ and $y-$ axis displacements. Conventional PI controllers require $d-q$ axis current in the rotor synchronous reference frame. Hence, the $d-q$ axis reference currents of each sector can be calculated multiplying $\bar{I}^*_{\alpha\beta}$ by an appropriate rotating matrix as in (8).

$$\bar{I}^*_{dq} = \mathbf{T}_R(\vartheta_e)\bar{I}^*_{\alpha\beta} \tag{8}$$

Where $\mathbf{T}_R(\vartheta_e)$ is defined in (9).

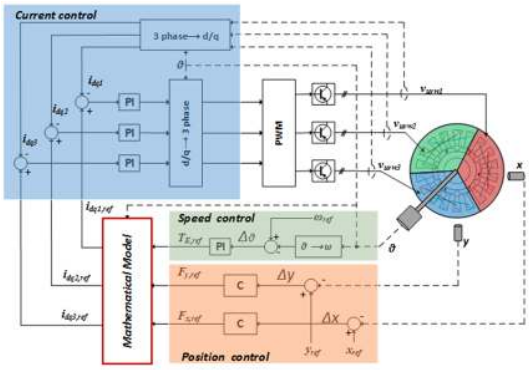

Fig. 3. Overall control scheme.

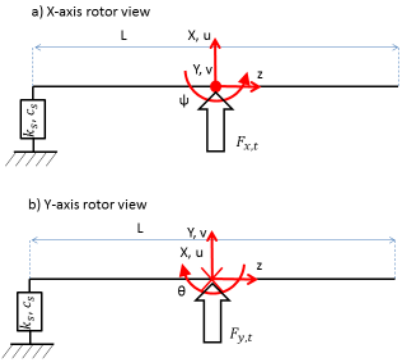

Fig. 4. Schematic representation of the rotor fixed to the self-alignment bearing and geometrical reference frame representation.

$$\boldsymbol{T}_R(\vartheta_e) = \begin{bmatrix} \mathbf{R}_{dq}(\vartheta_e) & \mathbf{0}_2 & \mathbf{0}_2 \\ \mathbf{0}_2 & \mathbf{R}_{dq}(\vartheta_e) & \mathbf{0}_2 \\ \mathbf{0}_2 & \mathbf{0}_2 & \mathbf{R}_{dq}(\vartheta_e) \end{bmatrix} \tag{9}$$

And $\mathbf{R}_{dq}(\vartheta_e) = \begin{bmatrix} \cos(\vartheta_e) & \sin(\vartheta_e) \\ -\sin(\vartheta_e) & \cos(\vartheta_e) \end{bmatrix}$.

III. 2-DOF Radial Position Control

This section deals with the design and tuning of the $x-y$ axis position controller. The overall control system can be represented in the block scheme of Fig. 3 where position and speed controller outputs are the inputs of the mathematical model block consisting of equations (7) and (8). Then, the mathematical model block output is the $d-q$ axis current vector $\bar{I}^*_{dq}$ consisting in $2n_s$ reference currents. In the MSPM motor considered $n_s = 3$ hence 3 independent $d-q$ axis current controllers are required, each of them controlling a standard three-phase inverter connected to the related motor sector.

A. The rotor dynamic system

In order to control 2-DOF the tilting movement and the axial displacement must be constrained by a self-alignment bearing mounted on one side of the shaft. The other side is free to move along the $x-y$ axis only. Fig. 4 presents a schematic of

the rotor system model showing the overall force acting on the mass centre and the $x-y$ axis reference frame positioned on it. The self-alignment bearing is modelled as a spring of stiffness k_s and a viscous damper c_s. Hence, assuming the rotor a rigid cylinder and considering small radial displacements, the suspension rotor dynamic system can be written in matrix form as follow [13]:

$$\mathbf{M}\ddot{\bar{q}} + \mathbf{G}\dot{\bar{q}} + \mathbf{K}\bar{q} = \bar{F} \tag{10}$$

where

$$\begin{aligned} \bar{q} &= \begin{bmatrix} u & v & \vartheta & \psi \end{bmatrix}^T \\ \mathbf{M} &= diag(m, m, J_d, J_d) \\ \mathbf{G} &= \begin{bmatrix} c_s & 0 & 0 & c_{s,c} \\ 0 & c_s & -c_{s,c} & 0 \\ 0 & -c_s & c_{s,r} & \omega J_p \\ c_s & 0 & -\omega J_p & c_{s,r} \end{bmatrix} \\ \mathbf{K} &= \begin{bmatrix} k_s & 0 & 0 & k_{s,c} \\ 0 & k_s & -k_{s,c} & 0 \\ 0 & -k_{s,c} & k_{s,r} & 0 \\ k_{s,c} & 0 & 0 & k_{s,r} \end{bmatrix} \\ \bar{F} &= \begin{bmatrix} F_{x,t} & F_{y,t} & 0 & 0 \end{bmatrix}^T \end{aligned} \tag{11}$$

$c_{s,c} = -Lc_s$, $k_{s,c} = -Lk_s$, $c_{s,r} = L^2 c_s$, $k_{s,r} = L^2 k_s$. $F_{x,t}$ and $F_{y,t}$ are the total $x-y$ forces described in (1) including a possible disturbance and, only in the $y-$axis, the rotor weight force. J_p and J_d are the polar and diametral moment of inertia of the rotor. ϑ and ψ are the angular rotation around the $x-$ and $y-$ axis, respectively. Their sign is chosen according to the conventions taken in Fig. 4. ω is the angular speed around the $z-$ axis. Being the ratio $J_p/J_d = 0.097$ and the maximum angular speed relatively low, the gyroscopic effect can be neglected. Furthermore, typical values of stiffness coefficients for ball bearings are $k_s = 110 \div 190$ [N/μm] therefore, the self-alignment bearing can by considered stiff. After the approximations introduced, the four equations of system (10) are decoupled and, for the position control purpose, only the first two are considered and written in (12).

$$\begin{bmatrix} m & 0 \\ 0 & m \end{bmatrix} \begin{bmatrix} \ddot{u} \\ \ddot{v} \end{bmatrix} - \begin{bmatrix} k_m & 0 \\ 0 & k_m \end{bmatrix} \begin{bmatrix} u \\ v \end{bmatrix} = \begin{bmatrix} F_{x,c} + F_{x,d} \\ F_{y,c} + F_{y,d} - mg \end{bmatrix} \tag{12}$$

$F_{x,c}$, $F_{y,c}$ and $F_{x,d}$, $F_{y,d}$ are the $x-y$ components of the forces generated by the controller and due to the disturbance, respectively. It is worth noting that system (12) has two unstable poles due to the presence of the magnetic stiffness constant that produces a force that tend to attract the rotor to the stator core.

B. The controller design

Since system (12) is decoupled, the position controller for the two axis can be designed separately. Fig. 5 shows the block scheme of the position controller structure chosen for both axis. p_{ref} and p stand for either $x-$ or $y-$ axis position reference and measure, respectively. Since the position controller main goal is to reject disturbances and keep the shaft

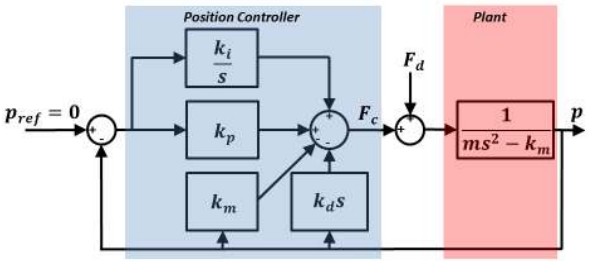

Fig. 5. Structure of the position controller.

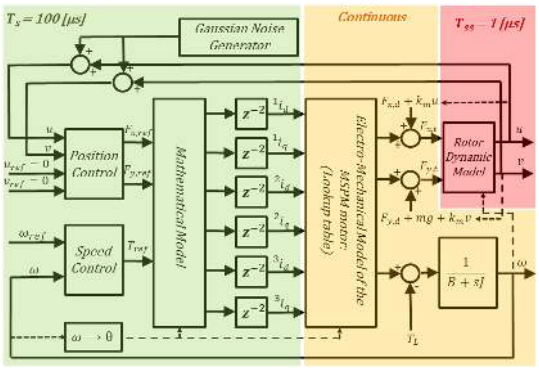

Fig. 6. Block scheme implemented in the MATLAB-Simulink environment.

centred, the closed loop transfer function from F_d to p has been analysed. The latter can be written as

$$T_{dp}(s) = \frac{1}{m} \frac{s}{s^3 + \frac{k_d}{m}s^2 + \frac{k_p}{m}s + \frac{k_i}{m}} \tag{13}$$

where k_p, k_i and k_d are the proportional, the integral and the derivative gain, respectively. k_m is considered as a known quantity and it is included in the position controller leading to the compensation to the PM force attraction. The controller parameters have been tuned using a pole placement technique, equating the denominator coefficients of (13) with those of the following polynomial.

$$\begin{aligned} &(s + \omega_c)(s^2 + 2\xi\omega_c s + \omega_c^2) = \\ &\quad = s^3 + (2\xi\omega_c + \omega_c)s^2 + (2\xi\omega_c^2 + \omega_c^2)s + \omega_c^3 \end{aligned} \tag{14}$$

ξ and ω_c are the desired damping ratio and pulsation of the final closed loop poles. Solving the resulting system of equations for the controller parameters, it results

$$\begin{cases} k_p = m\omega_c^2 (2\xi + 1) \\ k_i = m\,\omega_c^3 \\ k_d = m\omega_c (2\xi + 1) \end{cases} \tag{15}$$

IV. Simulation of the 2-DOF Levitation System

A. Simulation structure and set up

The block scheme of the simulation is shown in Fig. 6. It is possible to identify the $x-y$ position controller designed in the previous section and a standard PI controller for the

TABLE II
POSITION CONTROLLER GAINS

Parameter	Value
Proportional gain (k_p)	8.84e+06
Integral gain (k_i)	3.97e+09
Derivative gain (k_d)	7.04e+03

speed loop. Their outputs are the reference force components $F_{x,ref}$, $F_{y,ref}$ and the reference torque T_{ref}, respectively. The three quantities compose the vector $\bar{W}_E^*$ of the mechanical references that, together with the angular position ϑ_e, is the input of the mathematical model represented by the pseudo inverse matrix $\mathbf{K}_E^+$. The $d-q$ axis current references are then obtained as in (8). The current controllers of the $2n_s$ outputs of the mathematical model is represented by the block delays z^{-2} in the discrete domain. As a matter of fact, a well tuned current controller introduces a delay of two sample times T_s between the reference current and motor current (if no voltage saturation occurs).

The $d-q$ axis currents are the input of the block that includes the electro-mechanical model of the motor considered. The model is stored in the form of lookup table and it maps the $d-q$ axis currents to $x-y$ force components and torque. The lookup table has been carried out by mean "multi-static" non-linear FE simulations to take into account the iron saturation. In particular, for each angular rotor position the FE model of the motor has been fed with $d-$ axis and $q-$ axis currents ranging between $-I_n$ and I_n with steps of 1 [A]. Then, the matrix obtained has been imported in the MATLAB-Simulink model where a linear method has been employed for the interpolation of the lookup table elements. The rotor weight force, the open circuit force due to the rotor displacement and a possible disturbance are then added and the resultant $F_{x,t}$ and $F_{y,t}$ forces are the input of the rotor dynamic model block represented by equations (10). A Gaussian noise is summed to the position outputs to model the noise introduced by the displacement probes.

Both the position and speed controllers are implemented in the simulation in a discrete form, choosing as sample time value $T_s = 100[\mu s]$. The electro-mechanical model is simulated in continuous while the rotor dynamical model in discrete form with $1[\mu s]$ sample time.

B. Simulation results

At start-up the shaft leans on the backup bearing, hence, the starting position of the rotor in the coming simulations is $(0, -\delta_{max})$. The position controller parameters can be determined from equation (15) choosing a damping ratio of $\xi = 0.9$ in order to reduce oscillations. As a first approach, the simple block scheme of Fig. 5 is considered and ω_c is chosen in order to maintain a stable rotor suspension after a step disturbance equal to 95% of the nominal force $F_{max} = 200[N]$ is applied. The frequency obtained is 450 [Hz], defining the upper limit bandwidth of the control position considered in this work.

Afterwards, the simulation set up described by Fig. 6 is used in order to consider the discretized controllers, the motor saturation and the interaction between speed/position and current control loops. The latter causes the position to have a very big overshoot with a long damped oscillation, hence the bandwidth of the position controller needs to be reduced. The choice of the frequency is now a compromise between having stable suspension operations in the event of a force disturbance and a maximum overshoot of 20% of δ_{max} at start-up and after the disturbance is applied. The frequency chosen is 200 [Hz] allowing to stably suspend the rotor after a disturbance of 70% of F_{max} occurs. The position controller gains obtained are reported in Table II.

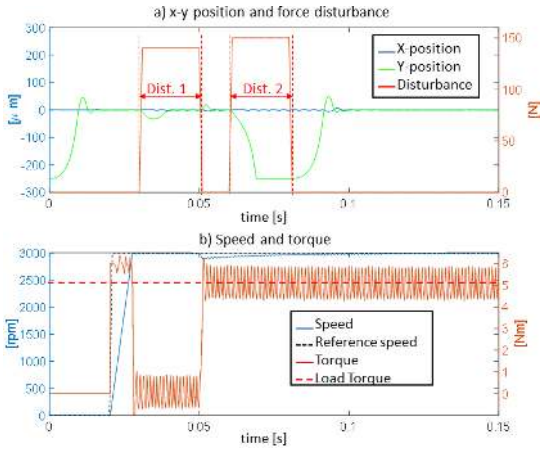

Fig. 7. Simulation result of the $x-y$ axis rotor position and speed control together.

The speed control PI is tuned in order to achieve a stable control. Fig. 7 a) shows that the rotor is kept centred after a disturbance of 140 [N] along the $y-$ axis is applied (the total disturbance is $140 + mg = 160[N]$) while it drops if the disturbance is higher. In the same simulation (Fig.7 b)) the speed reference step of 3000 [rpm] is commanded after the rotor is stabilized in the stator centre and a torque load step equal to the nominal torque $T_N = 5[Nm]$ is applied after $50ms$.

Finally, the rejection capability of the position control loop to sinusoidal force disturbances is investigated. This is particularly relevant since an eventual rotor unbalance or the unbalanced magnetic pull consists of periodic force disturbances with a frequency proportional to angular rotor speed. Fig. 8 shows the Bode diagram of the transfer function (13) with the parameters reported in Table II.

From Fig. 8, it is possible to notice that the most critical frequency is 146 [Hz]. Fig. 9 shows the simulative response of the system to a sinusoidal disturbance of frequency 146 [Hz] and amplitude 140 [N] applied on the $y-$axis between 0.03 and 0.1 [s]. The resulting position oscillation does not exceed 30% of the backup bearing clearance proving a good control performance. It is possible to observe from the figure that the $x-$ axis position is slightly affected by the disturbance on the $y-$ axis. This is caused by the increasing $x-$ axis force ripple due to the stator core saturation during the disturbance.

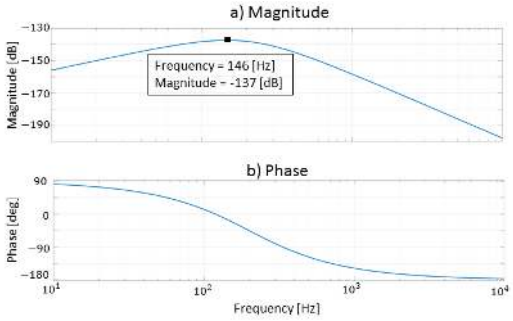

Fig. 8. Bode diagram of $T_{dp}(s)$

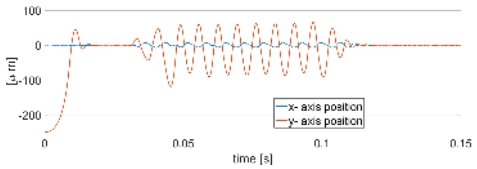

Fig. 9. $x - y$ axis position with sinusoidal disturbance.

C. FE validation of the numerical results

The lookup table of the electro-mechanical model in Fig. 6 has been carried out through FEA keeping the rotor centred. Hence, the validity of the simulation results obtained in the previous paragraph relies on the assumption that the forces and torque produced are not affected by the rotor displacement. The aforementioned assumption in general is false. However, the aim of this paragraph is to demonstrate that, within the displacement considered, the rotor radial position can be neglected in the force and torque production.
In order to do so, a simulation has been run adopting the same settings of Fig. 7 but without the disturbance of 150 [N] and the rotor angular and radial position and $d-q$ axis currents data has been saved. Then, a FE non linear "multi-static" simulation has been performed supplying the FE model with the data previously saved. The forces and torque generated by the FE simulation have been compared in Fig. 10 a)-b) with the output of the electro-mechanical model block of Fig. 6 showing a good agreement. Therefore, it is possible to conclude that, within the radial displacement considered, the aforementioned assumption is valid.

V. Conclusions

The radial force production principles of the MSPM machine considered has been discussed and described by a mathematical model. The rotor dynamic model of the rotor has been introduced and the position controller structure has been designed. The controller gains have been set in order to guarantee a stable rotor suspension when different force disturbances occur. The capabilities and performances of the proposed 2-DOF bearingless system are validated through MATLAB-Simulink simulations considering different kinds of force disturbances. It has been demonstrated that the position controller is capable to completely reject constant disturbances

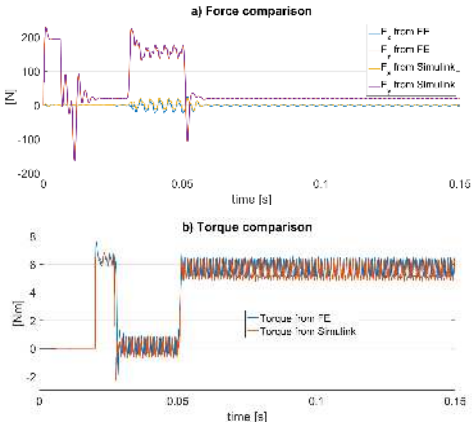

Fig. 10. Comparison of the suspension force and torque production between FEA and Simulink considering the rotor radial displacement.

and to stably suspend the rotor even when a sinusoidal disturbance at the critical frequency occurs
Finally, a further verification of the force and torque production has been done by mean FE simulations in order to consider a more truthful model of the machine.

References

[1] X. Sun, L. Chen, and Z. Yang, "Overview of bearingless permanent-magnet synchronous motors," *IEEE Transactions on Industrial Electronics*, vol. 60, no. 12, pp. 5528–5538, Dec 2013.

[2] T. Baumgartner, R. M. Burkart, and J. W. Kolar, "Analysis and design of a 300-w 500 x2009;000-r/min slotless self-bearing permanent-magnet motor," *IEEE Transactions on Industrial Electronics*, vol. 61, no. 8, pp. 4326–4336, Aug 2014.

[3] M. Ooshima, S. Kobayashi, and H. Tanaka, "Magnetic suspension performance of a bearingless motor/generator for flywheel energy storage systems," in *IEEE PES General Meeting*, July 2010, pp. 1–4.

[4] A. Chiba, T. Fukao, O. Ichikawa, M. Oshima, M. Takemoto, and D. G. Dorrell, *Magnetic bearings and bearingless drives*. Elsevier, 2005.

[5] P. K. Budig, "Article to the theory and application of magnetic bearings," in *International Symposium on Power Electronics Power Electronics, Electrical Drives, Automation and Motion*, June 2012, pp. 1526–1534.

[6] K. Inagaki, A. Chiba, M. A. Rahman, and T. Fukao, "Performance characteristics of inset-type permanent magnet bearingless motor drives," in *2000 IEEE Power Engineering Society Winter Meeting. Conference Proceedings (Cat. No.00CH37077)*, vol. 1, 2000, pp. 202–207 vol.1.

[7] W. K. S. Khoo and S. D. Garvey, "Practical implementation of the bridge configured winding for self-bearing machines," in *2005 Intern. Conf. on Power Electr. and Drives Systems*, vol. 2, Nov 2005, pp. 1146–1151.

[8] X. L. Wang, Q. C. Zhong, Z. Q. Deng, and S. Z. Yue, "Current-controlled multiphase slice permanent magnetic bearingless motors with open-circuited phases: Fault-tolerant controllability and its verification," *IEEE Trans. on Ind. Electr.*, vol. 59, no. 5, pp. 2059–2072, May 2012.

[9] S. Kobayashi, M. Ooshima, and M. N. Uddin, "A radial position control method of bearingless motor based on d - q -axis current control," *IEEE Trans. on Ind. Appl.*, vol. 49, no. 4, pp. 1827–1835, July 2013.

[10] G. Valente, L. Papini, A. Formentini, C. Gerada, and P. Zanchetta, "Radial force control of multi-sector permanent magnet machines," in *2016 XXII Inter. Conf. on Electr. Mach. (ICEM)*, Sept 2016, pp. 2595–2601.

[11] P. Bolognesi, "A mid-complexity analysis of long-drum-type electric machines suitable for circuital modeling," in *2008 18th International Conference on Electrical Machines*, Sept 2008, pp. 1–5.

[12] G. Valente, L. Papini, A. Formentini, C. Gerada, and P. Zanchetta, "Radial force control of multi-sector permanent magnet machines considering radial rotor displacement," in *2017 IEEE Workshop on Electr. Mach. Design, Contr. and Diagn. (WEMDCD)*, April 2017, pp. 140–145.

[13] M. I. Friswell, *Dynamics of rotating machines*. Cambridge University Press, 2010.